Interplay of slow bath fluctuations and energy transfer in 2D spectroscopy of the FMO light-harvesting complex: benchmarking of simulation protocols

Benoit Palmieri, Darius Abramavicius and Shaul Mukamel*

Recently developed approaches to simulate environment-induced fluctuation effects in two-dimensional (2D) spectroscopy of excitons are compared for the Fenna-Matthews-Olson light-harvesting complex. Fast fluctuations induce population redistribution between exciton energy-levels and raise homogeneous line widths of various peaks in 2D spectra. These effects are easily accounted for in sum-over-eigenstates (SOS) approach and the quasi-particle (QP) scattering approach through relaxation and dephasing rate constants. Slow fluctuations cause correlations of energies at various delay times in 2D photon-echo spectra. These may be calculated either by doing cumulant expansion in SOS techniques or by statistical averaging over static disorder in SOS and QP approaches. We compare the 2D photon-echo signal simulated using two levels of cumulant expansion approaches and two statistical averaging approaches for the same system. These levels differ by the treatment of energy-level correlations at different delay times and give rise to different cross-peak shapes: the cross-peaks retain their original diagonally elongated shapes when correlations are included, while they are more spherically broadened when correlations are neglected. Statistical averaging over disorder give very similar results but requires much higher computational effort. The peak redistribution timescales are very similar for all levels of theory. The spectral signatures at these different levels of theory are compared and simulation cost is estimated. Approaches which do require statistical averaging over disorder are orders of magnitude slower.

I. Introduction

Two-dimensional (2D) spectroscopy projects four-wave mixing signals onto frequency–frequency correlation plots that carry information on the structure and the dynamics of molecules and their interaction with the surrounding.[1] Of particular interest is the study of excited state coherent dynamics and population transport in chromophore aggregates.[2–8] Spectra are usually simulated using the nonlinear response formalism combined with simplified models for the excitation and solvent dynamics. Dynamical information on the environment is obtained from the peak line shape. Elliptical diagonally elongated peak patterns reflect the interplay of homogeneous and inhomogeneous broadening. Arbitrary timescales bath fluctuations can be calculated using the Cumulant Gaussian Fluctuations (CGF)[9,10] or the Redfield theory.[11,12] Static fluctuations can be included by repeated calculations to generate an ensemble.

Closed form approximate expressions for the femtosecond four-wave mixing of excitons were derived recently.[13] These expressions include slow diagonal fluctuations through a second order cumulant expansion; ensemble averaging is avoided. Two levels of approximation were proposed and

applied to simulate the response function of a model dimer including exciton transport. They assume different correlations between the slow bath coordinates. The first (here denoted sum over states SOS(A)) assumes an arbitrary degree of correlations between the slow diagonal bath coordinates but neglects the effects of the slow bath fluctuations on exciton transport. The second (SOS(B)) uses a single bath coordinate so that the slow diagonal fluctuations are fully correlated, but it is capable to include the Stokes shift. We shall compare them with two other levels of theory. The third level of theory is the standard CGF theory with static diagonal energy fluctuations incorporated by ensemble averaging (SOS(C)). The last level of theory is based on the quasiparticle representation (QP).[12,14,15] Ensemble averaging is still necessary, but the calculations of doubly-excited states is avoided. The difference between the four theories mainly resides in the way they deal with the slow fluctuations giving rise to inhomogeneous broadening.

In this paper, we report a benchmark comparison of these four levels of theory by applying them to the FMO light-harvesting antenna.[16,17] In section II, we briefly survey the advantages and cost of the four level of theories. In section III, we apply them to the photon echo $k_I = -k_1 + k_2 + k_3$ signal. We study the effect of the correlation between the slow bath coordinate and their effect on transport during the delay t_2 and we compare the numerical cost. Section IV contains a discussion along with some concluding remarks.

University of California at Irvine, 1102 Natural Sciences 2, Irvine, California 92697-2025, USA. Tel: 949-824-7600;
E-mail: smukamel@uci.edu

II. Theory

The aggregate is described by the Frenkel exciton Hamiltonian,[18,19]

$$\hat{H} = \sum_m \varepsilon_m \hat{B}_m^\dagger \hat{B}_m + \sum_{mn} J_{mn} \hat{B}_m^\dagger \hat{B}_n + \frac{\Delta}{2} \sum_m \hat{B}_m^\dagger \hat{B}_m^\dagger \hat{B}_m \hat{B}_m \tag{2.1}$$

where $\hat{B}_m^\dagger$ ($\hat{B}_m$) Pauli operators create (annihilate) an excitation on site (or chromophore) m. They obey the boson commutation relation,

$$[\hat{B}_m, \hat{B}_m^\dagger] = \delta_{nm}, \tag{2.2}$$

where δ_{mn} is the Dirac delta function. ε_m is the excited state energy of site m and J_{mn} is the coupling between sites. The Hamiltonian parameters (ε and J) for the FMO complex are given in ref. 4,20. The energy-shift is chosen such that the aggregate is modelled as coupled two-level systems, $\Delta \to \infty$.

The coupling with the bath has the form,

$$\hat{H}_{SB} = -\sum_m \hat{Q}_m \hat{B}_m^\dagger \hat{B}_m \tag{2.3}$$

where $\hat{Q}_m$'s are collective harmonic bath coordinate operators which cause population transport and line broadening. Each bath coordinate is characterized by its spectral density,[12]

$$C_\alpha''(\omega) = \frac{1}{2} \int dt\, e^{i\omega t} \langle [\hat{Q}_m(t), \hat{Q}_m(0)] \rangle, \tag{2.4}$$

which has the overdamped Brownian oscillator form,[12]

$$C_\alpha''(\omega) = 2\lambda_\alpha \frac{\omega \Lambda_\alpha}{\omega^2 + \Lambda_\alpha^2}. \tag{2.5}$$

λ controls the strength of the coupling with the bath and Λ^{-1} is the relaxation time-scale of the bath correlations. Derivations of the four approximations for the response function expressions can be found in ref. 9,11,13. In all cases, the homogeneous broadening and population transport are included by coupling each chromophore to its own, fast bath coordinate and Redfield theory (within the secular approximation) is used to describe population transport.[12,21]

The induced polarization is expressed as a convolution of the three incoming, time-resolved, pulses with the third order response function as follows,

$$\begin{aligned} \mathbf{P}^{(3)}(\mathbf{r},t) &= \int_0^\infty dt_3 \int_0^\infty dt_2 \int_0^\infty dt_1\, R^{(3)}(t_3, t_2, t_1) \\ &\quad E(\mathbf{r}, t - t_3)\, E(\mathbf{r}, t - t_3 - t_2 - t_1) \end{aligned} \tag{2.6}$$

where t_1, t_2 and t_3 are the time intervals between successive interactions with the electric field, E. The detected third-order signal is proportional to the third-order induced polarization, $P^{(3)}$, and is generated in the directions $\pm \mathbf{k}_1 \pm \mathbf{k}_2 \pm \mathbf{k}_3$. All the system (molecule and the solvent) information is contained in the response function, $R^{(3)}$.

The $\mathbf{k}_I = -\mathbf{k}_1 + \mathbf{k}_2 + \mathbf{k}_3$ signal is given as a sum of three terms represented by the Feynman diagrams shown in Fig. 1. These are denoted, "ground state bleaching" (GSB), "excited state emission" (ESE) and "excited state absorption" (ESA). The rules for these diagrams are given in ref. 12.
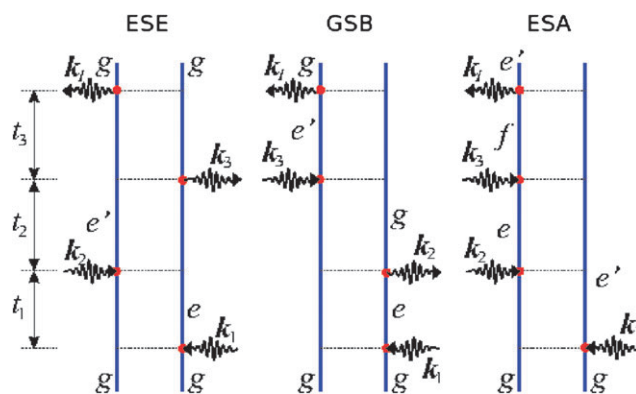

Fig. 1 The Feynman diagram representation of the three Liouville-space pathways contributing to the $\mathbf{k}_I$ response function. The three distinct pathways are denoted as Ground State Bleaching (GSB), Excited State Emission (ESE) and Excited State Absorption (ESA).

A. Sum-over-states with uncorrelated slow fluctuations [SOS(A)][13]

Here, we assume that each site is coupled to its own slow (but not necessarily static) bath coordinate. These coordinates are uncorrelated. Population transport during t_2 is described by a Pauli master equation. The population rates are not affected by the slow coordinate. The effects of the slow fluctuations on the propagation during t_2 which causes dynamic Stokes shift is thus neglected. The effect of the slow fluctuations on the response function is incorporated by a second order cumulant expansion. The response function is given by eqn (19) and (20) in ref. 13. It can be used for arbitrary bath time-scales, it includes fluctuation correlations between the time intervals t_1 and t_3 and ensemble averaging is avoided.

B. Sum-over-states with correlated slow fluctuations [SOS(B)][13]

This is similar to SOS(A) except that a single slow bath coordinate is coupled to all chromophores. Slow bath fluctuations are thus fully correlated and the dynamic Stokes shift is incorporated. The Pauli master equation describing population transport holds, since the population rate matrix is not modulated by the slow fluctuations. The resulting response function is given by eqn (29) and (30) in ref. 13 (or by eqn (164) and (179) in ref. 12). As in SOS(A), inhomogeneous broadening is incorporated without explicit ensemble averaging.

C. Sum-over-states with static fluctuations [SOS(C)][9]

Here, correlations of fluctuations between t_1 and t_3 are neglected. The response function is given by eqn (176) and (177) in ref. 12. Only fast bath fluctuations are included. By adding diagonal disorder to the Hamiltonian and ensemble averaging, the population transport rates are modulated by static disorder. The explicit ensemble averaging makes this procedure time-consuming compared to the previous two methods. This model has the same long t_2 limit as SOS(B) when bath correlations completely decay.

This journal is © the Owner Societies 2010

Phys. Chem. Chem. Phys., 2010, **12**, 108–114 | 109

D. The Quasi-particle representation [QP][11]

The fourth level of theory is fundamentally different from the sum over states methods. Excitation dynamics is described in terms of quasiparticles. This allows us to avoid the memory expensive computation of the doubly-excited eigenstates, which grows fast with the system size. The response function is expressed in terms of one-exciton Green's function and a scattering matrix. The advantages of the quasiparticle representation are explained in ref. 12, 22. Briefly, the response function is obtained by solving a hierarchy of differential equations starting with the Heisenberg equation for the time-evolution of the expectation value of the polarization operator. These Nonlinear Exciton Equations (NEE) are closed by retaining terms contributing up to third order in an expansion of the response function in the external fields. The $\mathbf{k}_I$ response function is given by eqn (124) of ref. 12. Population transport is calculated using the Redfield theory with the secular approximation[12] which decouples populations and coherences. Both the population transport and homogeneous dephasing are calculated in the Markovian approximation. This level of theory neglects all correlations between fluctuations in the t_1, t_2 and t_3 time intervals. It uses an even more restrictive approximation compared to the SOS methods; it assumes infinitely fast bath (Markovian) dynamics. Slow bath diagonal fluctuations are added to the Hamiltonian and the response function by averaging over many realizations of the diagonal disorder.

III. Numerical results

We have performed a benchmark comparison of the 4 computation methods applied to the FMO light-harvesting complex (Fig. 2).[16] The system consists of seven two-level chromophores embedded in a protein matrix. FMO is an excellent candidate for our benchmarking because the available model system parameters reproduce the experiment quantitatively.[4,5,20,23,24]

The following parameters were used:

(1) SOS(A): Each Chlorophyll is coupled to uncorrelated bath coordinates with $\Lambda_{\text{fast}}^{-1} = 75$ fs and $\lambda_{\text{fast}} = 35$ cm^{-1}. Inhomogeneous broadening is included by an additional set of uncorrelated bath coordinates with $\Lambda_{\text{slow}} \approx 0$ and with a system bath coupling of $\lambda_{\text{slow}} = 33.75$ cm^{-1}.
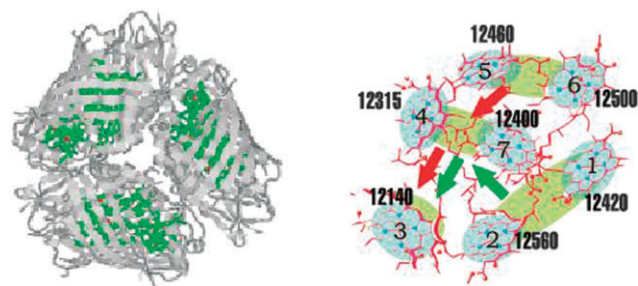

Fig. 2 The FMO light-harvesting system. Left panel: a trimer where each member has 7 chromophores is shown with the embedding proteins. Right-panel: the 7 chromophores and their excitation energies.

(2) SOS(B): Same as method SOS(A), but inhomogeneous broadening is included by adding another set of $\Lambda_{\text{slow}} \approx 0$ slow correlated bath coordinates with a system bath coupling of $\lambda_{\text{slow}} = 10.0$ cm^{-1}.

(3) SOS(C) and QP: Each Chlorophyll is coupled to one type of uncorrelated bath coordinates all having $\Lambda_{\text{fast}}^{-1} = 75$ fs and a system bath coupling $\lambda_{\text{fast}} = 35$ cm^{-1}. Inhomogeneous broadening is included by uncorrelated Gaussian diagonal disorder ($\sigma = 60$ cm^{-1}) to the Hamiltonian and ensemble averaging over 500 realizations.

$\Lambda_{\text{fast}}^{-1} = 100$ fs and $\lambda_{\text{fast}} = 55$ cm^{-1} with static diagonal disorder of $\sigma = 20$ cm^{-1} were used in ref. 20 using the SOS(C). For these parameters, inhomogeneous broadening is smaller
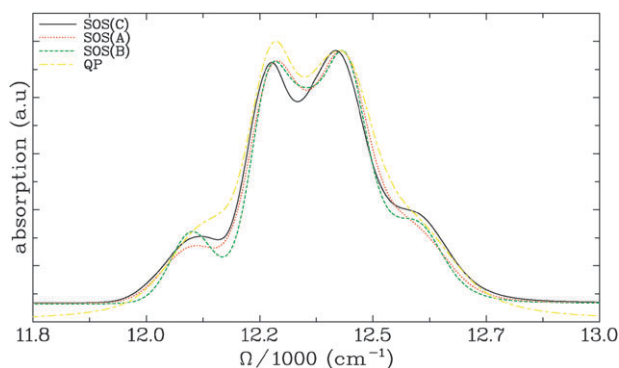

Fig. 3 Linear absorption spectra for the FMO light-harvesting complex calculated using the four levels of theory described in the text. All curves are normalized using the peak around 12 400 cm^{-1}. The line shapes predicted with the first three methods are similar. The SOS(A) and SOS(B) methods agree very well with each other and with SOS(C) in the regions of the two dominant peaks (between 12 200 and 12 500 cm^{-1}). SOS(A) agrees very well with SOS(C) in the low energy shoulder region ($\approx 12\,100$ cm^{-1}) and SOS(B) agrees very well with SOS(C) in the high energy shoulder region ($\approx 12\,600$ cm^{-1}). The broadening that results from the QP is slightly too large. This results from the Markov approximation which is used to calculate the line shapes in the QP.
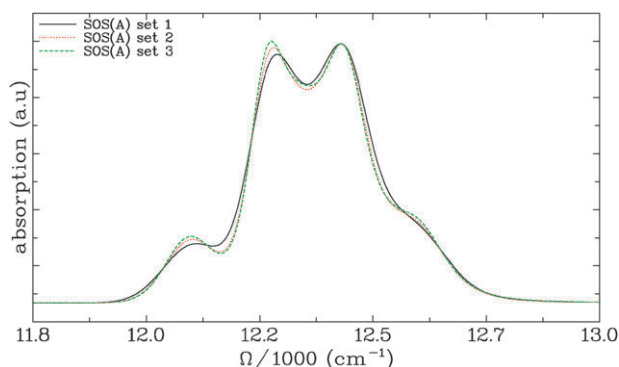

Fig. 4 Linear absorption spectra for the FMO light-harvesting complex calculated using the SOS(A) level of theory with different bath coupling parameters. In set 1, $\lambda_{\text{fast}} = 55$ cm^{-1} and $\Lambda_{\text{fast}}^{-1} = 106$ fs while $\lambda_{\text{slow}} = 5$ cm^{-1}. In set 2, $\lambda_{\text{fast}} = 45$ cm^{-1} and $\Lambda_{\text{fast}}^{-1} = 90$ fs while $\lambda_{\text{slow}} = 16$ cm^{-1} and in set 3, $\lambda_{\text{fast}} = 35$ cm^{-1} and $\Lambda_{\text{fast}}^{-1} = 75$ fs while $\lambda_{\text{slow}} = 32.65$ cm^{-1}. From set 1 to set 3, the importance of inhomogeneous broadening increases while the linear spectrum displays only small changes.

than homogeneous broadening. We used a different set of parameters which reproduce the experimental linear absorption and 2D spectra equally well, but whose inhomogeneous and homogeneous contributions to the line broadening are comparable. Simple approximate relations that connect λ_{slow} with variance σ can be derived for $\Lambda_{\text{slow}} \rightarrow 0$ by analyzing the various line broadening expressions of SOS(A), SOS(B) and SOS(C) given in ref. 13,12:

$$\lambda_{\text{slow}}(u) = \frac{\sigma^2}{2k_B T}$$
$$\lambda_{\text{slow}}(c) = \frac{\sigma^2}{6k_B T}$$

(3.1)

where $\lambda_{\text{slow}}(u)$ ($\lambda_{\text{slow}}(c)$) refers to the uncorrelated (correlated) slow bath coupling. These expressions were used to estimate

the couplings used in SOS(A) and SOS(B) and correspond to the static (ensemble averaging) fluctuations given by $\sigma = 60$ cm^{-1} in SOS(C) and QP.

The absorption spectra are shown in Fig. 3. The agreement with experiment (see ref. 4) is very good, except for the QP, which shows larger line broadening. This is a consequence of the Markovian approximation. It overestimates the broadening for the $\Lambda_{\text{fast}}^{-1} = 75$ fs bath coordinate.

In Fig. 4, SOS(A) is used for three sets of bath coupling parameters that give very similar absorption spectra. Set 1 reproduces the set of parameters used in ref. 20. Here, $\lambda_{\text{fast}} = 55$ cm^{-1} and $\Lambda_{\text{fast}}^{-1} = 106$ fs while $\lambda_{\text{slow}} = 5$ cm^{-1}. For this set of parameters, homogeneous broadening dominates. In set 2, $\lambda_{\text{fast}} = 45$ cm^{-1} and $\Lambda_{\text{fast}}^{-1} = 90$ fs while $\lambda_{\text{slow}} = 16$ cm^{-1}. This choice increases the inhomogeneous broadening. Set 3 is the one that was used in Fig. 3 (SOS(A)): $\lambda_{\text{fast}} = 35$ cm^{-1} and

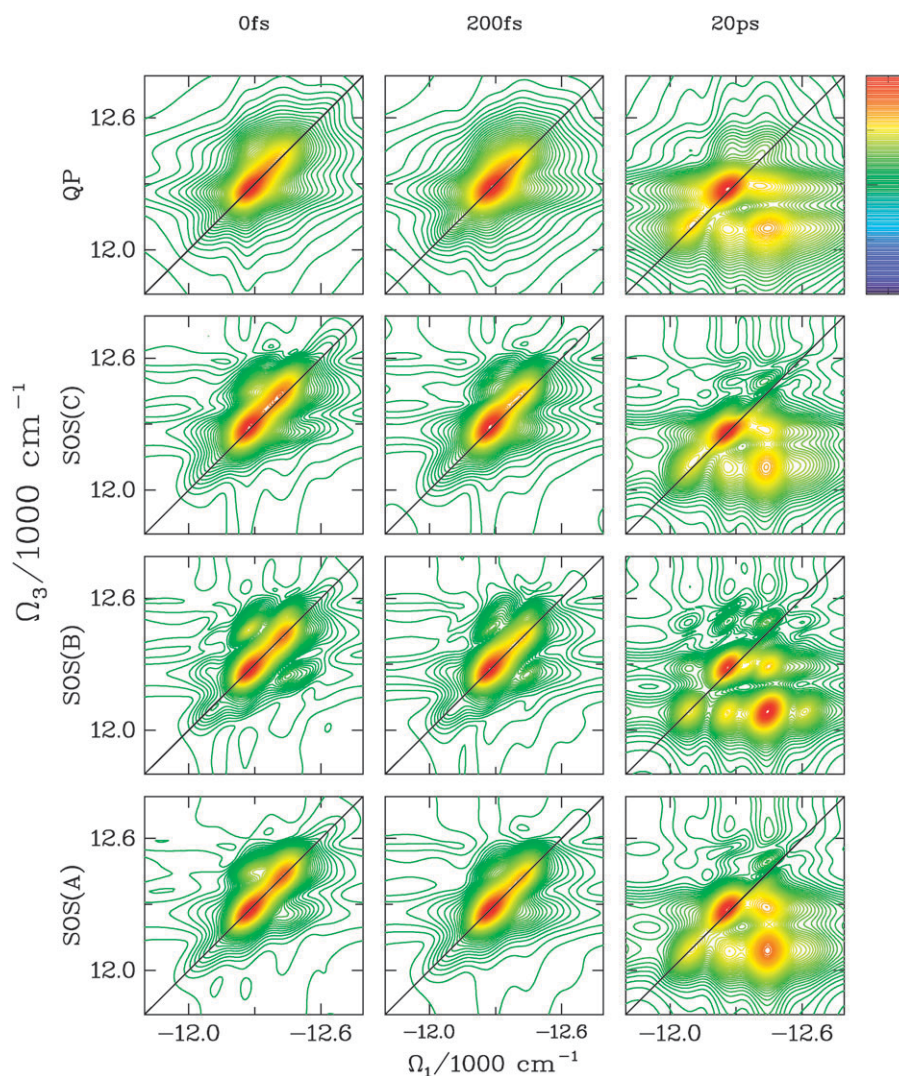**Fig. 5** The $\mathbf{k}_I$ spectra (absolute value) of FMO for $t_2 = 0$ fs, 200 fs and 20 ps is reported for the 4 different transport theories. At $t_2 = 0$ fs, the QP and SOS(B) differ from SOS(A) and SOS(C) which are very similar. The QP peaks are more broad whereas the dominant crosspeak in SOS(B) has a larger amplitude and is elongated along the diagonal. At $t_2 = 200$ fs, only the QP gives qualitatively different results (broader peaks). At $t_2 = 20$ ps, all theories capture the main features, but some finer details are different. The SOS(C) and SOS(A) techniques are quite similar in peak shapes although the intensity of the strongest cross peak is slightly larger in SOS(A). In SOS(B), the cross-peaks are elongated along the diagonal (the cross-peaks in SOS(A) and SOS(C) have a more circular shape) due to the correlated slow bath coordinate. In the QP, the diagonal peak is still too broad and the cross-peaks are similar to SOS(A) and SOS(C) but are slightly more elongated along Ω_1.

This journal is © the Owner Societies 2010

Phys. Chem. Chem. Phys., 2010, **12**, 108–114 | 111

$\Lambda_{\text{fast}}^{-1} = 75$ fs while $\lambda_{\text{slow}} = 32.65$ cm^{-1}. The differences between the absorption spectra calculated with the three sets of parameters is rather small, highlighting that such fits are not unique. Hereafter, we focus solely on set 3, where inhomogeneous broadening is the largest.

The photon echo $\mathbf{k}_I = -\mathbf{k}_1 + \mathbf{k}_2 + \mathbf{k}_3$ spectra for short and large t_2 are displayed in Fig. 5. SOS(A) and SOS(B) simulations are at least 500 times faster than SOS(C) and $\sim$100 times faster than the QP. All theories essentially show the same features at $t_2 = 0$ and $t_2 = 200$ fs. The QP has slightly larger homogeneous broadening (elongation of the peaks across the diagonal). The weak cross-peak that appears above the diagonal for SOS(A) and SOS(C) is stronger for correlated slow bath coordinate (SOS(B)). The $t_2 = 20$ ps spectra show that, in all cases, the peak redistribution due to population transport occurs on very similar timescales, but the shapes of the peaks are different. The cross-peaks have an elongated shape in SOS(B), but are roughly circular in all other cases. This is not surprising because no matter where the excitations are transported after t_2, the correlations between

t_3 and t_1 are the same because of the fully correlated nature of the fluctuations. Hence, the line broadening of the redistributed off-diagonal peaks is expected to have the same elongated shape as the $t_2 = 0$ diagonal peaks. For uncorrelated fluctuations, the correlation between t_1 and t_3 vanish for long t_2 and the cross-peaks become circular.

In Fig. 6, we use the pulse polarization configurations described in ref. 20 to separate the coherence dynamics from the population. Using the symmetry of the population pathways, the combination of $R_{\mathbf{k}_I,xyyx} - R_{\mathbf{k}_I,xyxy}$ eliminates population contributions to the signal; only coherence contributions remain.[20] From the top, the first and third row of Fig. 6 show $R_{\mathbf{k}_I,xyyx} - R_{\mathbf{k}_I,xyxy}$ for SOS(B) and SOS(A), respectively. Coherences decay at similar timescales in both cases, but the difference in peak shapes is more evident in this representation.

The other two rows show the results of the technique $R_{\mathbf{k}_I,xyyx} - R_{\mathbf{k}_I,xxyy}$ which, by symmetry, cancels the ESE coherent contributions to the signal.[20] The remaining population peaks redistribute in a very similar manner and
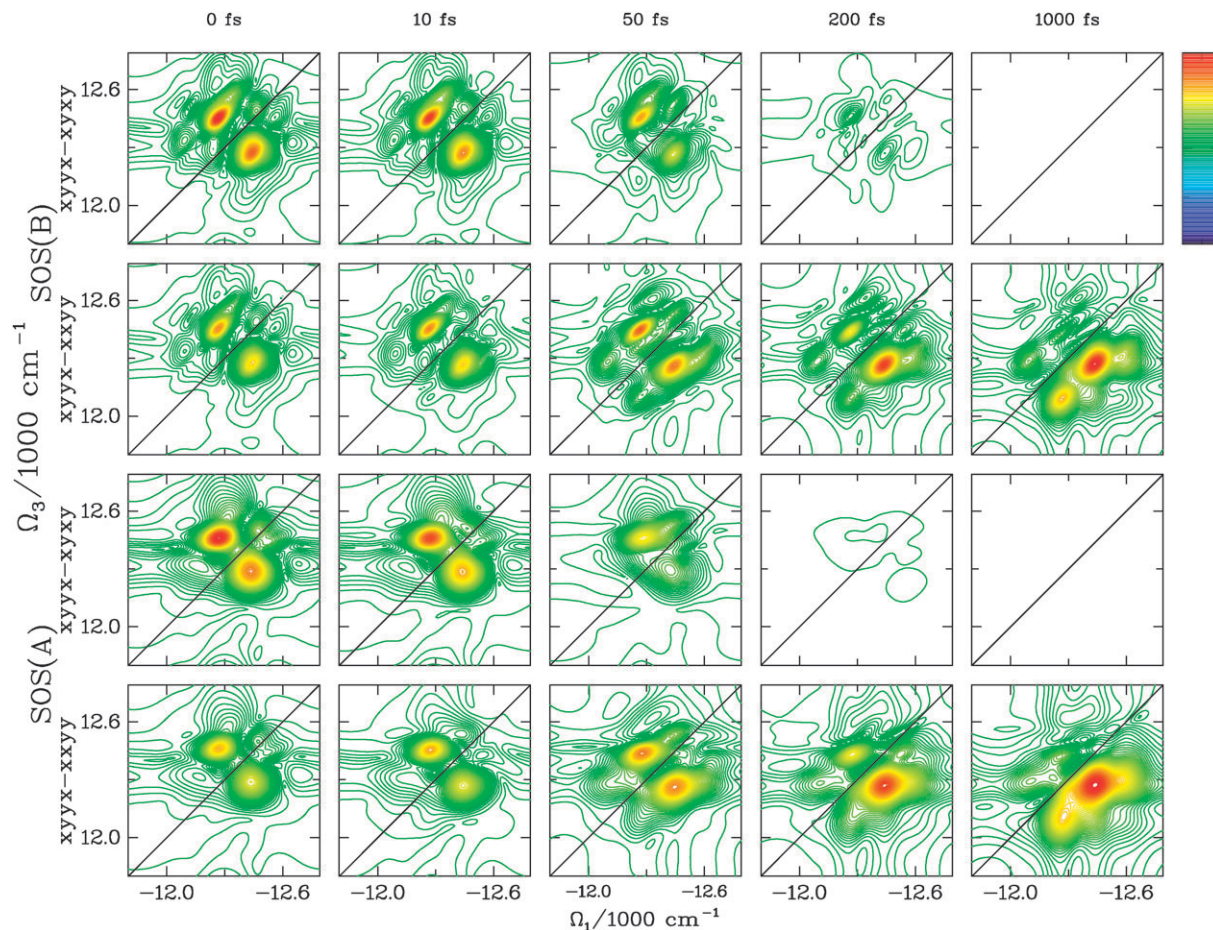

Fig. 6 We compare the signal $R_{\mathbf{k}_I,xyyx} - R_{\mathbf{k}_I,xyxy}$ that eliminates population contributions and the signal $R_{\mathbf{k}_I,xyyx} - R_{\mathbf{k}_I,xxyy}$ that eliminates the coherent contributions to the ESE Liouville space pathway for the two transport theories SOS(A) (uncorrelated bath, bottom two rows) and SOS(B) (correlated bath, top two rows). We consider the following t_2: 0 fs, 10 fs, 50 fs, 200 fs, 1000 fs. Obviously, the coherent dynamics decays on a much faster timescale. The shape of the peaks differs when the slow bath coordinate is correlated or uncorrelated. Again, for correlated bath, the peaks are elongated along the diagonal. Furthermore, the coherent dynamics decay on a faster timescale for the uncorrelated case. For the signal that probes the population ($R_{\mathbf{k}_I,xyyx} - R_{\mathbf{k}_I,xxyy}$), we observe the same features as in Fig. 5, the peaks redistribute with the same timescale for both transport theories and they appear elongated along the diagonal for the correlated case.

Table 1 Summary of the four level of theories with their pros and cons. The running time required to calculate the response function shown in Fig. 5 with SOS(C) on an average speed computer is about 2 days

Theory	Fast bath correlations	Slow bath correlations	Explicit Ens. Averaging	Speedup (*cf* to SOS(C))	Pros and cons
SOS(A)	any	any	no	500	Pros: fast calculation Cons: No Dynamic Stokes shift, approximate population rates
SOS(B)	any	correlated	no	500	Pros: fast calculation, Dynamic Stokes shift included, exact population rates Cons: Slow bath must be fully correlated
SOS(C)	any	any	yes	1	Pros: Exact population rates, arbitrary disorder Cons: Time-consuming
QP	any	any	yes	5	Pros: Scales favorably with system size, exact population rates, arbitrary disorder Cons: Time-consuming

with the same time-scale for SOS(B) and SOS(A). Again, the peak shapes are strongly affected by the correlation of the bath.

In summary, the simulations shown in Fig. 6 highlight the difference in peak shapes predicted by the different theories at a finer level (by selecting specific Liouville-space pathways) and shows that the short-time scale under which the cross-peaks evolve is again very similar for SOS theories.

IV. Discussion

The present benchmark simulations show that SOS(A) and SOS(B) give very similar results for the $\mathbf{k}_I$ signal for all t_2's considered (0–20 ps). Only the shape of the cross-peaks differ when the slow bath coordinate is correlated (SOS(B)). The predicted peak redistribution due to population transport is quantitatively similar for all levels of theory even when the effect of inhomogeneous broadening on transport is completely neglected (SOS(A)); an approximation that appears to be justified in the light of these results. The QP peak line shapes are too broad, indicating that the Markovian regime does not apply for the fast bath coordinate with $\Lambda_{\text{fast}}^{-1} = 75$ fs. SOS(A) allows any level of correlations for the bath coordinates. SOS(B) requires fully correlated slow fluctuations. To compare the two, we chose the fluctuations to be completely uncorrelated in SOS(A). To include partially correlated fluctuations, SOS(A) must be used.

A technique with improved resolution that combines various signals to compare specific Liouville-space pathways (Fig. 6) shows that the shorter coherent lifetimes are almost identically predicted by different theories. Again, at these shorter time-scales, only the peak shapes differ because of the differences in the slow bath correlations. Fig. 6 shows that smaller amplitude peaks that are not observable in Fig. 5 also evolve in a very similar manner for both levels of theory.

SOS(A) and SOS(B) are superior since they cut down the computation time by two-orders of magnitude compared with SOS(C). These protocols require a large memory due to the explicit calculation of doubly-excited states in sum-over-states methods. Truncation procedures in the scattering matrix calculation make the QP to scale-more favorably with system size, but it requires explicit ensemble averaging for static fluctuations.

Our benchmark study is summarized in Table 1. For small aggregates, where computer memory is of no concern, SOS(A) and SOS(B) represent a very appealing and efficient procedure to simulate response functions. They reproduce the results of more expensive calculations, allow the inclusion of correlation for the bath coordinates and require significantly shorter running times. Note that the actual running time for simulating the SOS(C) response function in Fig. 5 on an average speed computer is about 2 days.

We have chosen a system where inhomogeneous and homogeneous broadening contributions to the response function are similar (set 3 in Fig. 4) and observed only small differences in the predicted spectra for all t_2. When the homogenous broadening dominates (set 1 in Fig. 4), we expect an even stronger agreement with SOS(C). Moreover, SOS(A), which neglects the effects of inhomogeneous broadening on transport, will then be more adequate.

References

1 S. Mukamel, *Principles of Nonlinear Optical Spectroscopy*, Oxford University Press, New York, 1995.
2 H. van Amerongen, L. Valkunas and R. van Grondelle, *Photosynthetic Excitons*, World Scientific, Singapore, 2000.
3 B. Gobets and G. R. van Grondelle, *Biochim. Biophys. Acta, Bioenerg.*, 2001, **1507**, 80.
4 T. Brixner, J. Stenger, H. M. Vaswani, M. Cho, R. E. Blankenship and G. R. Fleming, *Nature*, 2005, **434**, 625.
5 G. S. Engel, T. R. Calhoun, E. L. Read, T. K. Ahn, T. Mančal, Y. C. Cheng, R. E. Blankenship and G. R. Fleming, *Nature*, 2007, **446**, 782.
6 R. J. Cogdell and C. Mullineaux, *Photosynth. Res.*, 2008, **95**, 117.
7 H. Lee, Y.-C. Cheng and G. R. Fleming, *Science*, 2007, **316**, 1462.
8 D. Zigmantas, E. L. Read, T. Mančal, T. Brixner, A. T. Gardiner, R. J. Cogdell and G. R. Fleming, *Proc. Natl. Acad. Sci. U. S. A.*, 2006, **103**, 12672.
9 W. M. Zhang, T. Meier, V. Chernyak and S. Mukamel, *J. Chem. Phys.*, 1998, **108**, 7763.
10 D. Abramavicius and S. Mukamel, *Chem. Rev.*, 2004, **104**, 2073.
11 V. Chernyak, W. M. Zhang and S. Mukamel, *J. Chem. Phys.*, 1998, **109**, 9587.
12 D. Abramavicius, B. Palmieri, D. V. Voronine, F. Šanda and S. Mukamel, *Chem. Rev.*, 2009, **109**, 2350.
13 D. Abramavicius, L. Valkunas and S. Mukamel, *Europhys. Lett.*, 2007, **80**, 17005.
14 F. Spano and S. Mukamel, *Phys. Rev. A: At., Mol., Opt. Phys.*, 1989, **40**, 5783.

15 S. Mukamel, R. Oszwaldowski and D. Abramavicius, *Phys. Rev. B: Condens. Matter Mater. Phys.*, 2007, **75**, 245305.
16 R. Fenna and B. Matthews, *Nature*, 1975, **258**, 573.
17 W. B. R. A. J. Li and Y.-F. Zhou, *J. Mol. Biol.*, 1997, **271**, 456.
18 A. Davydov, *Theory of Molecular Excitons*, McGraw-Hill, New York, 1962.
19 E. Rashba and M. Sturge, *Excitons*, Elsevier, New York, 1987.
20 D. Abramavicius, D. V. Voronine and S. Mukamel, *Biophys. J.*, 2008, **94**, 3613.
21 B. Palmieri, D. V. Abramavicius and S. Mukamel, *J. Chem. Phys.*, 2009, **130**, 204512.
22 W. Zhuang, T. Hayashi and S. Mukamel, *Angew. Chem., Int. Ed.*, 2009, **48**, 3750.
23 R. J. W. Louwe, J. Vrieze, A. J. Hoff and T. J. Aartsma, *J. Phys. Chem. B*, 1997, **101**, 11280.
24 S. Vulto, M. de Baat, R. Louwe, H. Permentier, T. Neef, M. Miller, H. van Amerongen and T. Aartsma, *J. Phys. Chem. B*, 1998, **102**, 9577.